IET Generation, Transmission & Distribution

Special Issue: Challenges and New Solutions for Enhancing Ancillary Services and Grid Resiliency in Low Inertia Power Systems

Provision of inertial response as ancillary service from active distribution networks to the transmission system

ISSN 1751-8687
Received on 9th April 2020
Revised 7th July 2020
Accepted on 28th July 2020
E-First on 9th September 2020
doi: 10.1049/iet-gtd.2020.0675
www.ietdl.org

Álvaro Rodríguez del Nozal[1], Eleftherios O. Kontis[2,3], Juan M. Mauricio[1], Charis S. Demoulias[2] ✉

[1]*Department of Electrical Engineering, Universidad de Sevilla, Seville, Spain*
[2]*School of Electrical and Computer Engineering, Aristotle University of Thessaloniki, Thessaloniki, Greece*
[3]*Department of Electrical and Computer Engineering, University of Western Macedonia, Kozani, Greece*
✉ *E-mail: chdimoul@auth.gr*

Abstract: Nowadays, traditional synchronous generators are replaced by distributed renewable energy sources (DRESs), which are connected to the grid via power converters. This shift towards non-synchronous generation leads to low inertia power systems and affects considerably the frequency control procedure. To provide an inertial response and to enhance grid stability, DRESs can be equipped with fast discharging energy storage systems, such as ultracapacitors. This feature allows distribution system operators (DSOs) to provide an inertial response as ancillary service to transmission system operators (TSOs) by coordinating the operation of many DRESs. For this purpose, DSOs should develop tools to quantify and control the provision of inertial response. Towards this objective, in this study, two new methodologies are proposed. The first one aims to evaluate the maximum aggregated inertial capability of active distribution networks (ADNs). The second one aims to dispatch DRESs to provide specific, TSO-defined, inertial response with the minimum cost. Both methods are tested on a medium voltage grid. Several cases are examined highlighting the impact of different parameters, such as converter limitations, line congestions, on the inertial capability of ADNs. Results indicate that the proposed methods can fully exploit operational limits of ADNs and maximise their inertial capability.

1 Introduction

The power system industry is increasingly moving towards generating electricity from distributed renewable energy sources (DRESs) [1, 2] that are connected to the utility grid via power electronic converters [3, 4]. Indeed, in several regions around the world, such as South Australia, Hawaii, Texas and Tasmania, 50–60% of the local load is covered during specific time instants from DRESs [3]. A similar situation is also foreseen for the European system in the near future. Specifically, according to [5] it is expected that until the year 2025 generation from DRESs will cover at least 50% of the instantaneous power demand in 22 European countries. In countries such as Denmark, Germany, Great Britain, Greece, Ireland, Netherlands and Portugal, this percentage will reach up to the level of 100%.

1.1 Low inertia power systems

As the penetration of converter-interfaced DRESs increases, more and more conventional synchronous generators (SGs) are disconnected from the utility grid. This shift towards non-conventional non-synchronous generation changes notably the dynamic properties of modern power systems, jeopardising the overall system stability [4, 6]. A recent report, published by the European Network of Transmission System Operators for Electricity (ENTSO-E), has ranked the reduction of total system inertia as the most important power system stability challenge for the European system [7]. Similar remarks are also presented in [8], where a survey among 21 European transmission system operators (TSOs) is performed to identify the most critical stability challenges as perceived by the power system industry.

In the near future, several national TSOs in Europe will face frequency stability issues due to the significant reduction of the system inertia caused by the decommissioning of conventional SGs [4, 5]. Specifically, it is expected that until 2030 in Great Britain, Ireland, Italy, Greece, Northern Europe and Iberian peninsula the overall inertia constant during specific time instants will fall below 2 s (compared to traditional values ranging between 5 and 6 s) [4]. In this context, ENTSO-E has established the 'Technical Group on High Penetration of Power Electronic Interfaced Power Sources' to determine technical solutions that will enhance system stability.

As discussed in several reports of this Technical group [4, 9] as well as in several research papers [10–13], one emerging solution to the above-mentioned stability issues is the interconnection of DRESs to the utility grid via grid-forming converters [3]. The operation of grid-forming converters is fundamentally different compared to the conventional grid-following converters that are mainly used nowadays for the interconnection of DRESs [10, 12]. Grid-following converters are controlled as current sources either in a grid-parallel mode or in a grid-supporting mode of operation. In the former, converters do not change their power injections with respect to grid changes [10]. Therefore, they cannot provide an inertial response to the power system. In the grid-supporting mode, converters measure the frequency and voltage of the grid using a phase-locked loop and adapt their injected currents to feed the grid with the desired active and reactive power [12]. Thus, to provide an inertial response, grid-supporting converters first need to measure grid frequency and then modify their active power injections accordingly. On the other hand, in the grid-forming mode converters are controlled as voltage sources, targeting to establish and maintain the grid voltage and frequency [10, 12]. In this case, the power response of the converters is a direct consequence of network frequency perturbations. Thus, grid-forming converters can provide true inertia to the power system as required in [4].

Several grid-forming implementations, based on voltage source converters (VSCs), have been proposed in the literature [14–16]. The common characteristic of all these approaches is that an energy buffer, such as a battery storage system or an ultracapacitor (UC), is used to provide an inertial response to the grid [3, 11]. The inertial response of VSCs is fully programmable and tunable [17, 18], while the corresponding inertia constants can be adjusted even remotely by the system operator [16].

1.2 Motivation and scope of the paper

The above-mentioned unique characteristics will allow distribution system operators (DSOs) to create and manage portfolio of DRESs in order to provide inertial response as ancillary service (AS) to the transmission system [19]. However, to achieve this objective, a number of open issues must be solved.

More specifically, as explained in [4], it is still unclear if VSCs, connected to medium voltage (MV) active distribution networks (ADNs), can provide significant amounts of inertial response to the transmission grid without jeopardising the distribution system security and reliability. Other limiting factors may include the protection systems that are currently used in distribution systems [4], the economics associated with the size of the energy storage system [3] as well as the converter limits [12].

Scope of the paper is to develop new tools and methods that will allow DSOs to overcome the above-mentioned shortcomings and limitations, facilitating this way the provision of inertial response from ADNs to the transmission grid. Towards this objective, two new algorithms are proposed.

The first algorithm is based on an optimal power flow (OPF) formulation and aims to compute the maximum inertial capability of ADNs. Note, that the maximum inertial capability is defined in this paper as the maximum power that can be offered at the point of common coupling (PCC) with the transmission grid, without violating network limits. These limits include voltage and current limits, UCs limitations as well as temperature limitations of power converters. Voltage and current limits, as well as UC limitations are included as constraints in the proposed OPF formulation, while a thermal model of VSCs is introduced to take into account converter temperature limitations.

The second algorithm is also based on an OPF formulation and aims to optimally coordinate the operation of many DRESs in order to provide specific levels of inertial response at the PCC with the transmission grid. These levels can be agreed in advance with the TSO. To efficiently coordinate the operation of the DRESs, DSO should take into account all grid technical constraints, described in the previous paragraph.

The proposed algorithms are tested on the European MV benchmark grid introduced by CIGRE in [20]. Several tests cases and scenarios are considered, including different demand and generation levels as well as different sizes for the energy storage systems. The analysis of the results provides useful insights and a better understanding concerning the capability of ADNs to provide an inertial response at the transmission system.

Following this introduction, the remaining of the paper is organised as follows: in Section 2, the theoretical background is presented to set the notation for the rest of the paper. Specifically, grid constraints, limitations of energy storage systems and temperature limitations of power converters are discussed. In Section 3, current and future trends concerning the provision of inertial response are discussed. Additionally, a framework is presented for the interaction and communication between the TSO and DSOs. Scope of the framework is to facilitate the provision of inertial response from DSOs to the TSO. The developed algorithms are presented and explained in detail in Sections 4 and 5. The proposed methods are evaluated in Section 6. Finally, Section 7 summarises the findings of the research and concludes the paper.

2 Theoretical background

In this paper, all DRESs are assumed to be interconnected to the distribution grid via VSCs. Additionally, each DRES is equipped with an UC, the energy of which is used to provide a true inertial response to the grid during frequency events. Note that UCs are used in this paper as storage systems since they can be used to provide also other ASs to the transmission system [19], e.g. high-frequency power smoothing, injection of controllable fault currents etc.

To facilitate the reading of the paper, the theoretical background is discussed in this Section. Specifically, modelling of ADNs and the related technical and operational constraints are presented in Section 2.1. Section 2.2 presents the modelling of DRESs and discusses constraints related to the operation of UCs. Finally, Section 2.3 introduces the thermal model, used to evaluate temperature limitations of power converters.

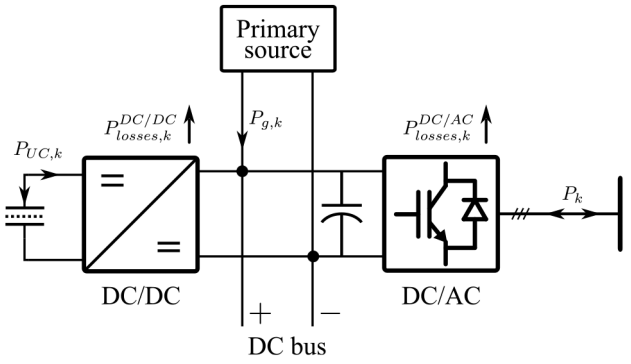

Fig. 1 *Structure of DRES*

2.1 Modelling of ADNs

ADNs are connected to the transmission grid via interconnection transformers. For their modelling, in this paper, the undirected graph $\mathcal{G} = (\mathcal{V}, \mathcal{E})$ is used. Here, $\mathcal{V} = \{0, 1, \ldots, p\}$ denotes the set of buses of the ADN. Without loss of generality, it is assumed that the interconnection transformer is placed between buses 0 and 1. Here, bus 0 denotes the high voltage side of the transformer at the head of the whole distribution network, while bus 1 the MV side. $\mathcal{E} \subseteq \mathcal{V} \times \mathcal{V}$ represents the set of power lines between the network buses. Additionally, $\mathcal{N}_i := \{j\colon (j,i), (i,j) \in \mathcal{E}\}$ is used to denote the neighbourhood of bus i, i.e. the set of buses that are connected to bus i. Finally, $\mathcal{D}_i = \{1, 2, \ldots, d_i\}$ is used to declare the set of DRESs that are connected to bus i.

The following set of equations is used to simulate the operation of the ADN:

$$\sum_{k \in \mathcal{D}_i} \mathcal{S}_k - \mathcal{S}_i^{\mathrm{L}} = \sqrt{3}\,\mathcal{U}_i \mathcal{I}_i^*, \quad \forall i \in \mathcal{V} \tag{1}$$

$$\sum_{j \in \mathcal{N}_i} \mathcal{I}_{i,j} = \mathcal{I}_i, \quad \forall i \in \mathcal{V}, j \in \mathcal{N}_i \tag{2}$$

$$\mathcal{U}_i - \mathcal{U}_j = \mathcal{Z}_{i,j} \mathcal{I}_{i,j}, \quad \forall i \in \mathcal{V}, j \in \mathcal{N}_i \tag{3}$$

Here $\mathcal{S}_i^{\mathrm{L}}$ is the complex load demand at bus i, while $\mathcal{S}_k$ denote the complex power of the kth DRES at bus i. Furthermore, $\mathcal{U}_i$ and $\mathcal{I}_i$ denote the complex phase-to-phase voltage and the complex current injection at bus i, respectively. Additionally, $\mathcal{I}_{i,j}$ denote the current flowing through line (i,j), while $\mathcal{Z}_{i,j}$ is the impedance of the corresponding line. Note that $\mathcal{Z}_{i,j} = \mathcal{Z}_{j,i}$ and $\mathcal{I}_{i,j} = -\mathcal{I}_{j,i}$.

To ensure the secure and reliable operation of the ADN, bus voltages and line currents should remain within pre-defined limits, as shown below:

$$V^{\min} \leq \left|\mathcal{U}_i\right| \leq V^{\max}, \quad \forall i \in \mathcal{V} \tag{4}$$

$$\left|\mathcal{I}_{i,j}\right| \leq I_{i,j}^{\max}, \quad \forall i \in \mathcal{V},\ j \in \mathcal{N}_i \tag{5}$$

here $V^{\max}$ and $V^{\min}$ are the upper and lower voltage limits, respectively, while $I_{i,j}^{\max}$ denotes the maximum ampacity of the line.

2.2 Modelling of DRESs

The structure of a VSC-interfaced DRES is presented in Fig. 1. As shown, the DRES consists of an UC and two power converters. The power coming from the primary source in DC form is converted to AC form by means of a VSC converter. The UC is connected to the DC-link by means of a DC/DC bidirectional buck–boost converter. When an under-frequency event occurs, the UC provides the power that must be injected to the grid. This

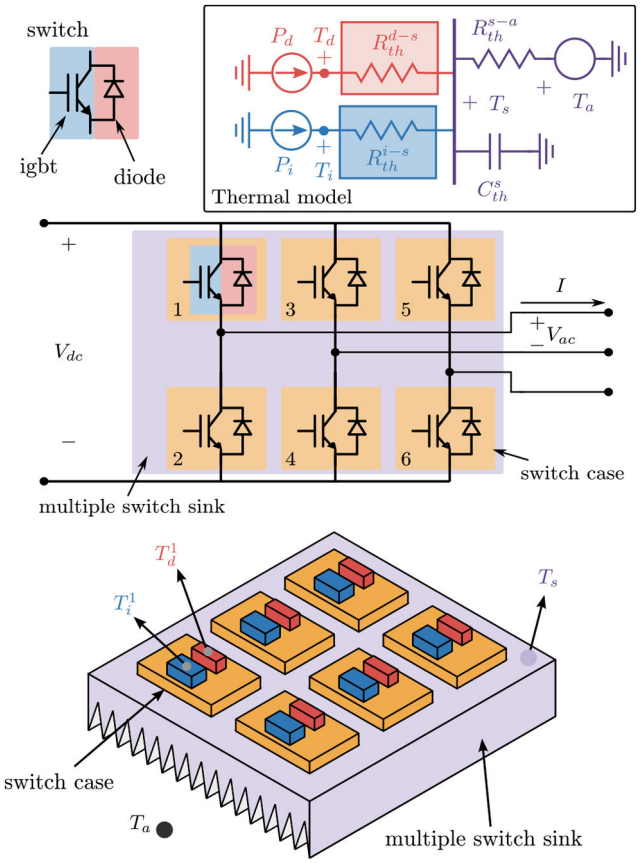

Fig. 2 *Single heatsink-based converter*

power flows through the DC/DC converter and the DC/AC converter and finally injected into the grid in AC form.

The reactive power of the kth DRES is determined by the adopted voltage control scheme, while the real power injection of the kth DRES can be written as

$$P_k = P_{g,k} + P_{\mathrm{UC},k} - P^{\mathrm{DC/DC}}_{\mathrm{losses},k} - P^{\mathrm{DC/AC}}_{\mathrm{losses},k} \tag{6}$$

where P_k denotes the total injected active power of the kth DRES. $P_{g,k}$ is the power provided by the primary source, while $P_{\mathrm{UC},k}$ is the power provided by the UC. Additionally, $P^{\mathrm{DC/DC}}_{\mathrm{losses,k}}$ and $P^{\mathrm{DC/AC}}_{\mathrm{losses},k}$ are the power losses during the DC/DC and DC/AC power conversion, respectively. Further information concerning $P_{\mathrm{UC},k}$, $P^{\mathrm{DC/DC}}_{\mathrm{losses},k}$ and $P^{\mathrm{DC/AC}}_{\mathrm{losses},k}$ are provided in the next Subsections.

2.2.1 Constraints of UCs: The power provided by the UC during a frequency event can be evaluated using the swing equation [21]

$$\Delta P(\mathrm{pu}) = 2H\frac{\mathrm{d}f}{\mathrm{d}t}\frac{1}{f_{\mathrm{n}}} \tag{7}$$

here $\mathrm{d}f/\mathrm{d}t$ is the rate of change of frequency (ROCOF). f_{n} is the nominal frequency of the grid, while H is the inertia constant. Given the fact that the UC do not provide power to the grid prior to the frequency event, (7) can be rewritten as

$$P_{\mathrm{UC},k}(\mathrm{pu}) = 2\tilde{H}_k\frac{\mathrm{d}f}{\mathrm{d}t}\frac{1}{f_{\mathrm{n}}} \tag{8}$$

where $\tilde{H}_k$ denote the inertia constant used for the sizing of the UC. Limitations for the UCs can be summarised as

$$P_{\mathrm{UC},k} \le P^{\max}_{\mathrm{UC},k} \tag{9}$$

$$P_{\mathrm{UC},k} \le \frac{3600E^{\max}_{\mathrm{UC},k}\mathrm{SoC}_{\mathrm{UC},k}}{\tilde{H}_k} \tag{10}$$

In the above notation, $P^{\max}_{\mathrm{UC},k}$ denotes the maximum discharging power of the UC. $P^{\max}_{\mathrm{UC},k}$ can be computed, in pu, if the maximum ROCOF withstand capability of the DRES is considered in (8). $P^{\max}_{\mathrm{UC},k}$ can be converted to kW using as base power the rated power of the DRES, i.e. S_{n}. Additionally, $\mathrm{SoC}_{\mathrm{UC},k}$, expressed in pu, is the state of charge of the UC, while $E^{\max}_{\mathrm{UC},k}$ denotes the energy capacity that the UC must have in order to provide $P^{\max}_{\mathrm{UC},k}$ power for $\tilde{H}_k$ seconds. $E^{\max}_{\mathrm{UC},k}$ is defined as

$$E^{\max}_{\mathrm{UC},k} = \frac{\tilde{H}_k}{3600}P^{\max}_{\mathrm{UC},k} \tag{11}$$

Division with 3600 is used to convert the inertia constant from seconds to hours. If $\mathrm{SoC}_{\mathrm{UC},k} = 1$, then (10) coincides with (9).

2.3 Modelling of power converters

In this section the electrothermal model used to compute power losses of the converters as well as the temperature of their constitutive components, is presented. The proposed model follows the widespread approach considered by the most important manufacturers [22–24] and is summarised in [25].

2.3.1 Converter power losses: Converter power losses can be computed as

$$P_{\mathrm{i}}(I) = \Theta\left[a_{\mathrm{i}} + (b_{\mathrm{i}} + c_{\mathrm{i}}\alpha)I + (d_{\mathrm{i}} + e_{\mathrm{i}}\alpha)I^2\right] \tag{12}$$

$$P_{\mathrm{d}}(I) = \Theta\left[a_{\mathrm{d}} + (b_{\mathrm{d}} + c_{\mathrm{d}}\alpha)I + (d_{\mathrm{d}} + e_{\mathrm{d}}\alpha)I^2\right] \tag{13}$$

where P_{i} and P_{d} are the individual power losses for each IGBT and diode, respectively, represented as a function of the output RMS current I. The parameter α is defined as the product of the power converter modulation index (m) and the corresponding power factor, i.e. $\alpha = m\cos\phi$. Additionally, Θ represents the quotient between the transient heatsink temperature, T_{s}, and its steady-state value, $T^{\mathrm{ss}}_{\mathrm{s}}$. The computation of T_{s} is discussed in more detail in the next Subsection. The rest of the coefficients, i.e. $C = [a_{\mathrm{i}}, b_{\mathrm{i}}, c_{\mathrm{i}}, d_{\mathrm{i}}, e_{\mathrm{i}}, a_{\mathrm{d}}, b_{\mathrm{d}}, c_{\mathrm{d}}, d_{\mathrm{d}}, e_{\mathrm{d}}]$, can be obtained following the methodology in [25].

In this paper, we assume that the DC/AC converter is composed of six switches, while the DC/DC bidirectional buck–boost converter consists of two switches. Thus, the associated power losses can be computed as

$$P^{\mathrm{DC/AC}}_{\mathrm{losses},k} = 6(P_{\mathrm{i}}(|\mathcal{I}_k|) + P_{\mathrm{d}}(|\mathcal{I}_k|)) \tag{14}$$

$$P^{\mathrm{DC/DC}}_{\mathrm{losses},k} = 2(P_{\mathrm{i}}(|\mathcal{I}_{\mathrm{UC},k}|) + P_{\mathrm{d}}(|\mathcal{I}_{\mathrm{UC},k}|)) \tag{15}$$

here I_k denotes the output current at the AC side of the kth VSC, while $\mathcal{I}_{\mathrm{UC},k}$ is the current at the UC side.

2.3.2 Temperature limitations: The most important limitation, concerning the power that can be provided by a converter, is related to the maximum temperature of its constitutive components. Indeed, the temperature of IGBTs and diodes is limited according to a maximum permissible temperature $T^{\max}$ as shown below

$$T_{\mathrm{igbt}} \le T^{\max}, \quad T_{\mathrm{d}} \le T^{\max} \tag{16}$$

To take into account these limitations, the thermal model of (17)–(19) is introduced. To better explain the model, Fig. 2 is used, where a possible power converter arrangement is presented. In this arrangement, each pair of IGBT and diode is mounted on a case.

The cases, that are represented in Fig. 2 with yellow colour, are placed on a common heatsink.

The IGBT and diode juncture temperatures can be calculated as follows [25]

$$T_{\mathrm{i}} = T_{\mathrm{s}} + P_{\mathrm{i}} R_{\mathrm{th}}^{\mathrm{i-s}}, \tag{17}$$

$$T_{\mathrm{d}} = T_{\mathrm{s}} + P_{\mathrm{d}} R_{\mathrm{th}}^{\mathrm{d-s}}, \tag{18}$$

where $R_{\mathrm{th}}^{\mathrm{i-s}}$ and $R_{\mathrm{th}}^{\mathrm{d-s}}$ are the respective thermal resistances between their junctures and the heatsink with temperature T_{s} that is modelled with the following first order differential equation:

$$\frac{\mathrm{d}T_{\mathrm{s}}}{\mathrm{d}t} = \frac{1}{C_{\mathrm{th}}^{\mathrm{s}}}\left(N_{\mathrm{s}}(P_{\mathrm{igbt}} + P_{\mathrm{d}}) - \frac{T_{\mathrm{s}} - T_{\mathrm{a}}}{R_{\mathrm{th}}^{\mathrm{s-a}}}\right) \tag{19}$$

here N_{s} is the total number of switches cases on the heatsink, while C_{th} is the equivalent thermal capacitance of the heatsink. For more details about this thermal model and a methodology for obtaining the parameters refer to [25].

3 Provision of inertia from ADNs

3.1 Current and future trends

As the decommissioning of conventional SGs increases, the total system inertia decreases, leading to higher ROCOF values. However, large ROCOF values jeopardise the secure system operation for several reasons. Activation of ROCOF protection relays and mechanical limitations of conventional SGs can be considered as the most important ones [26]. Therefore, TSOs should ensure that the ROCOF remains always within permissible limits [26].

To achieve this, TSOs should ensure that total system inertia remains always at high levels. However, nowadays, system inertia becomes highly variable due to the intermittent nature of DRESs [27]. Therefore, to estimate the total system inertia, required to restrict ROCOF within permissible limits, TSOs conducts contingency analysis based on normative incidents [26, 28] (usually the tripping of the largest generating facility). If contingency analysis reveals that total system inertia is significantly low, corrective actions are applied, e.g. substitution of low inertia power sources by high-inertia power sources (thermal power plants) [9] or use of synchronous compensators [27]. However, these approaches are rather expensive [9, 27]. Hence, inertia markets are foreseen for the near future [19, 29, 30]. Under this concept, power producers, i.e. thermal power plants, wind- and PV-parks, compete with each other (through market mechanisms and price signals) to provide an inertial response as AS to the TSO [30].

Potentially, ADNs can also participate in future inertia markets. However, in order for this to happen, a number of technical barriers must be firstly addressed [19]. Indeed, nowadays, DRESs connected within ADNs are not 'visible' to TSOs, i.e. TSOs are completely unaware concerning the dynamic capabilities of these units. As a consequence, TSOs do not control the operation of DRES connected at the distribution level. Additionally, there are no methodologies to determine the total, i.e. aggregated, the contribution of ADNs to the inertial response.

A promising solution to overcome the above-mentioned barriers is to operate ADNs as virtual power plants (VPPs). To operate ADNs as VPPs and provide an inertial response as AS to the transmission system, DSOs shall coordinate the operation of many DRESs to perform the following tasks:

(i) Estimate the maximum additional power that can be delivered during a frequency event at the PCC with the transmission grid. This additional power is used to alleviate the system ROCOF. Thus, it can be considered as the maximum inertial capability of the ADN. To estimate this maximum additional power, DSO should take into account all technical and operational constraints to ensure the secure and reliable operation of the ADN.

(ii) Provide specific and TSO-defined inertial response. In a market-based environment, ADNs will compete with other market participants concerning the provision of inertial response as AS to the transmission system. In this framework, all market offers are evaluated in order to minimise the cost of the AS. Therefore, during specific time instants ADNs will reduce their share in the market, simply because other participants will provide more competitive bids. In these cases, TSOs should send appropriate dispatch signals to the corresponding ADNs to reduce their contribution to the inertial response, since they will not be remunerated for the extra power. Thus, DSOs should be able to coordinate the operation of many DRESs in order to provide this TSO-defined inertial response. To efficiently coordinate all DRESs, technical and operational constraints of ADN must be considered to ensure the secure and reliable operation of the grid.

3.2 Proposed framework

To operate ADNs as VPPs and to facilitate the implementation of the above-mentioned tasks, a centralised approach is developed in this paper. The proposed approach is depicted in Fig. 3 and it requires the interaction between TSO and DSOs. As shown, in predetermined time intervals Δt the TSO communicates with all DSOs. Generally, Δt is a TSO-defined parameter that can vary from a few minutes up to several hours. During the communication the TSO informs the DSOs concerning the maximum ROCOF, i.e. $\mathrm{ROCOF}_{\mathrm{max}}$ that DRESs shall at least be capable of withstanding [26]. Using this information, each DSO evaluates the maximum inertial capability of its ADN and estimates the cost of the corresponding AS. To quantify the maximum inertial capability of the examined ADN, the DSO should be able to estimate the maximum aggregated inertia constant of the ADN, i.e. $H_{\mathrm{ag}}^{\mathrm{max}}$.

To accomplish this, the DSO should initially calculate the power flowing through the PCC prior to the frequency disturbance. This is the pre-disturbance steady-state power and it is denoted as P_0^{ss}. Subsequently, DSO should take into account all technical and operational constraints of the ADN to estimate the maximum power that can be offered, during a frequency disturbance, at the PCC with the transmission grid. This power is denoted in this paper as P_0^{IRmax}. Afterwards, using P_0^{ss}, P_0^{IRmax} and $\mathrm{ROCOF}_{\mathrm{max}}$, the DSO computes $H_{\mathrm{ag}}^{\mathrm{max}}$. In particular, by performing some simple manipulations in (7) we obtain

$$H_{\mathrm{ag}}^{\mathrm{max}} = \frac{f_{\mathrm{n}}}{2}\frac{P_0^{\mathrm{IRmax}}(\mathrm{pu}) - P_0^{\mathrm{ss}}(\mathrm{pu})}{\mathrm{ROCOF}_{\mathrm{max}}} \tag{20}$$

Finally, the cost of the AS is estimated and the $H_{\mathrm{ag}}^{\mathrm{max}}$ value alongside with the corresponding cost are forwarded to the TSO.

As shown in Fig. 3, in the proposed framework, the TSO communicates with several DSOs to obtain the individual $H_{\mathrm{ag}}^{\mathrm{max}}$ values of all ADNs that are connected to the transmission system via interconnection transformers. Using the $H_{\mathrm{ag}}^{\mathrm{max}}$ values of all ADNs, the TSO conducts contingency analysis for the whole power system, using the framework presented in [28]. Contingency analysis may reveal that from a stability perspective it is not necessary all ADNs provide their maximum inertial response. In this case, the contribution of each ADN can be reduced to minimise the cost of the AS. To accomplish this, new inertia constants denoted as $H_{\mathrm{ag}}^{\mathrm{TSO}}$, are determined through market mechanisms and forwarded to the corresponding DSOs. Obviously, $H_{\mathrm{ag}}^{\mathrm{TSO}} < H_{\mathrm{ag}}^{\mathrm{max}}$. Once the DSOs receive the new settings for the aggregated inertia constants, should optimally dispatch DRESs that are connected to their network to ensure the required $H_{\mathrm{ag}}^{\mathrm{TSO}}$ value at PCC. To dispatch DRESs each DSO should determine the individual inertia constants, i.e. H_k, of all DRESs that are connected to its network.

As shown in Fig. 3, the above-mentioned procedure is repeated until the maximum number of time instants t_{max} has been reached.

The algorithms proposed in this paper to estimate the maximum inertial capability of the ADN and to optimally dispatch DRESs in

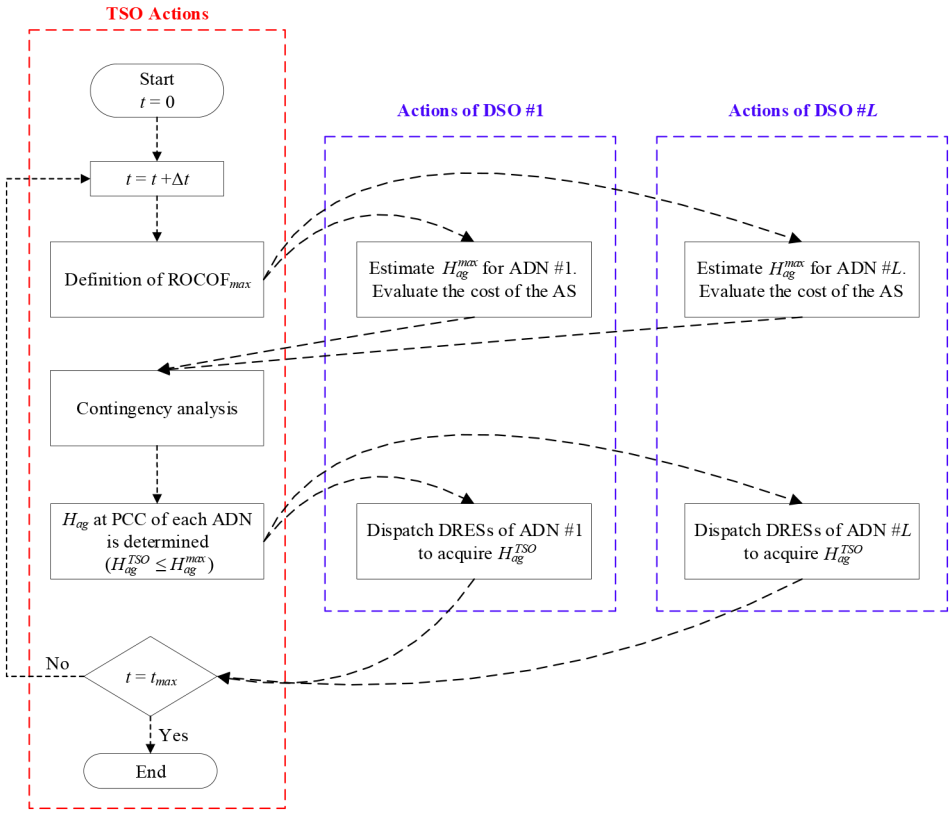

Fig. 3 *Interaction between DSOs and the TSO for the provision of inertial response. In this figure, L DSOs are considered. Each DSO is responsible for an ADN*

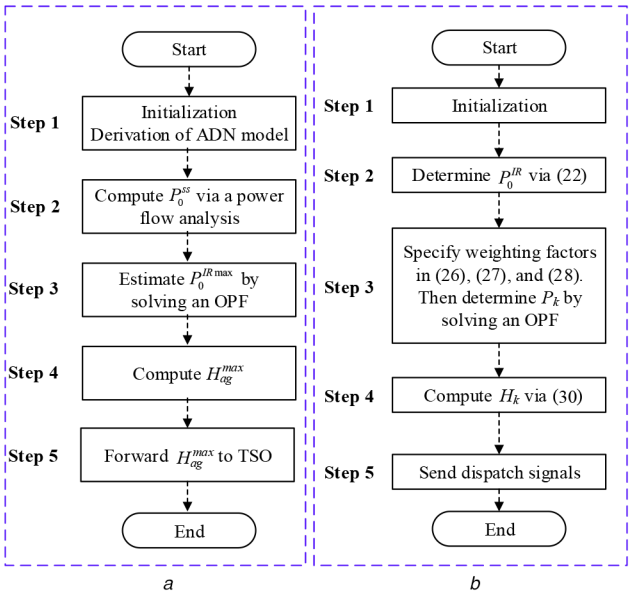

Fig. 4 *Proposed Algorithms*

(a) Algorithm 1: Methodology to estimate the maximum inertial capability of ADNs, ***(b)*** Algorithm 2: Methodology to dispatch DRESs in order to provide specific, TSO-defined, inertia constant at PCC

order to provide specific H_{ag}^{TSO} values are presented in Sections 4 and 5, respectively.

4 Evaluation of the maximum inertial capability of ADNs

The algorithm developed to estimate the maximum inertial capability of ADNs is depicted in Fig. 4*a* by means of a flowchart. The algorithm consists of five main steps as described in detail below:

Step 1. Initialisation phase: At this step, data related to the network topology, the rated power and the location of DRESs and loads as well as short-term load and generation forecasts are forwarded as inputs to the algorithm. Using these inputs, the model of the examined ADN is developed.

Step 2. Determination of the pre-disturbance steady-state power: Subsequently, using the model developed in step 1 and (1)–(3) a power flow calculation is performed to determine P_0^{SS}, i.e. the active power delivered at the PCC prior to the frequency disturbance. DRES active power injections that produce P_0^{SS} will be denoted for the rest of the paper as P_k^{SS}. Alternatively, P_0^{SS} can be measured using power loggers located at the interconnection transformer. If these measurements are available, they can also be used for the validation and the fine-tuning of the ADN model.

Step 3. Determination of the maximum inertial response: At this step, the DSO imposes all technical and operational constraints of the ADN. These constraints are expressed in (4), (5), (10) and (16) and refer to maximum network voltage and line current limits, to UC limitations and to temperature limits of converters, respectively. Once these constraints are specified, an OPF, expressed by (1)–(5), (10) and (16), is solved in Python using the minimise solver of Scipy library [31]. Power flow results of step 2 are used as the initial conditions of the OPF. The objective of the proposed OPF is to adjust the power injections of all DRESs, i.e. P_k and Q_k, in order to determine the maximum power, i.e. P_0^{IRmax}, that can be delivered during the inertial response at the PCC without violating technical and operational constraints. The objective function of the proposed OPF as well as the control variables are formally defined as

$$(\bar{P}^{\text{IRmax}}, \bar{Q}^{\text{IRmax}}) = \arg \max_{(\bar{P},\bar{Q})} \Re(\mathcal{U}_0 \mathcal{I}_{0,1}^{*}) \tag{21}$$

$\bar{P} = \{P_k, \forall k \in \mathcal{D}_i, \forall i \in \mathcal{V}\}$ and $\bar{Q} = \{Q_k, \forall k \in \mathcal{D}_i, \forall i \in \mathcal{V}\}$ are the sets of active and reactive powers of all DRESs. The super-index IRmax stands for the value of those power injections that maximise (21).

Step 4. Calculation of the aggregated inertia constant: At this step, the inertial capability of the examined ADN is quantified by computing the corresponding aggregated inertia constant, i.e. $H_{\text{ag}}^{\max}$. As already discussed, $H_{\text{ag}}^{\max}$ is computed using (20).

Step 5. Communication with the TSO: The value of $H_{\text{ag}}^{\max}$ is forwarded to the TSO and the algorithm terminates.

5 Optimal allocation of inertia

To dispatch DRESs in order to provide specific, TSO-defined, inertia constants at the PCC, the algorithm of Fig. 4*b* is proposed. The algorithm consists of five main steps, as described in detail below:

Step 1. Initialisation phase: At this step, the TSO-defined inertia constant, i.e. $H_{\text{ag}}^{\text{TSO}}$ and the $\text{ROCOF}_{\max}$ value are forwarded as inputs to the algorithm. Additional, inputs include the ADN model developed in step 1 of Algorithm 1 as well as short-term load and generation forecasts.

Step 2. Determination of the active power that should be released at the PCC during the inertial response: At this stage, the DSO determines the amount of active power that should be delivered at the PCC in order to obtain an aggregated inertia constant for the ADN equal to $H_{\text{ag}}^{\text{TSO}}$. This power is denoted as P_0^{IR} and can be calculated using (22). Note that (22) can be directly derived from (7) by performing some simple manipulations.

$$P_0^{\text{IR}}\,(\text{pu}) = 2H_{\text{ag}}^{\text{TSO}}\frac{1}{f_{\text{n}}}\text{ROCOF}_{\max} + P_0^{\text{ss}}\,(\text{pu}) \tag{22}$$

In (22), $H_{\text{ag}}^{\text{TSO}}$ and $\text{ROCOF}_{\max}$ are known parameters, defined by the TSO, while P_0^{ss} is calculated from the DSO as discussed in step 2 of Algorithm 1.

Step 3. Network optimisation: Once P_0^{IR} is computed, the remaining task focuses on the dispatch of the DRESs in order to determine individual power injections, i.e. P_k and Q_k, for all DRESs so as to achieve the P_0^{IR} power at the PCC. Ideally, the dispatch should target to minimise the cost of the AS. This actually requires detailed cost-functions quantifying the cost of the foreseen AS. To the authors best knowledge there are no related cost-functions in the literature. Thus, in this paper, the dispatch is performed using an OPF targeting to minimise (24). Following this approach, costs related with the grid operation, such as converter and line losses, are minimised. The proposed OPF is expressed by (1)–(5), (10) and (16). The objective function as well as the control variables to be determined are formally presented next

$$(\bar{P}^{\text{IR}}, \bar{Q}^{\text{IR}}) = \arg\min_{(P,\,Q)} C, \tag{23}$$

with

$$C = C_{\text{losses}}^{\text{lines}} + C_{\text{losses}}^{\text{DC/DC}} + C_{\text{losses}}^{\text{DC/AC}} + C^{\text{VD}}. \tag{24}$$

Recall that super-index *IR* stands for the value of those power injections that minimise the above cost function.

In the above equations, $C_{\text{losses}}^{\text{line}}$ denotes the total cost related with line losses variation due to the inertial response. $C_{\text{losses}}^{\text{DC,DC}}$ and $C_{\text{losses}}^{\text{DC,AC}}$ denote the total costs related with extra power losses during DC/DC and DC/AC power conversion, respectively, while C^{VD} denote the cost related with network voltage deviations. A detailed description of the above-mentioned cost terms is provided below

Line losses variation: The power provided by DRESs during the inertial response causes variation to network power losses. This variation can be estimated as

$$P_{\text{losses}}^{\text{lines}} = \sum_{(i,\,j)\,\in\,\mathscr{E}} R_{i,j}\left(\left|\mathscr{I}_{i,j}\right|^2 - \left|\mathscr{I}_{i,j}^{\text{ss}}\right|^2\right) \tag{25}$$

where $I_{i,j}^{\text{ss}}$ is the complex value of the current flowing through line (i, j) during the pre-disturbance steady-state operation, while $I_{i,j}$ is the line current during the inertial response. The total cost related with line losses is calculated in this paper as

$$C_{\text{losses}}^{\text{lines}} = w_{\text{losses}}^{\text{lines}} P_{\text{losses}}^{\text{lines}}, \tag{26}$$

here, $w_{\text{losses}}^{\text{lines}}$ is a weighting factor that is specified by the DSO. If $w_{\text{losses}}^{\text{lines}}$ is equal to zero, then line losses are not taken into account in (24).

Converter extra losses: The losses related with the DC/DC and DC/AC power conversion are calculated as

$$C_{\text{losses}}^{\text{DC/DC}} = w_{\text{losses}}^{\text{DC/DC}} \times \sum_{i\,\in\,\mathscr{V}} \sum_{k\,\in\,\mathscr{D}_i} 2\left(P_{\text{igbt}}\left(\left|\mathscr{I}_{\text{UC},k}\right|\right) + P_d\left(\left|\mathscr{I}_{\text{UC},k}\right|\right)\right), \tag{27}$$

$$C_{\text{extralosses}}^{\text{DC/AC}} = w_{\text{extralosses}}^{\text{DC/AC}} \times \sum_{i\,\in\,\mathscr{V}} 6\left(P_{\text{igbt}}\left(\left|\mathscr{I}_i\right| - \left|\mathscr{I}_i^{\text{ss}}\right|\right) + P_{\text{d}}\left(\left|\mathscr{I}_i\right| - \left|\mathscr{I}_i^{\text{ss}}\right|\right)\right), \tag{28}$$

where $\mathscr{I}_i^{\text{ss}}$ is the current injection at node i in steady-state operation prior to the disturbance. Here $w_{\text{losses}}^{\text{DC/DC}}$ and $w_{\text{losses}}^{\text{DC/AC}}$ are two weighting factors, adjusted by the DSO. If $w_{\text{losses}}^{\text{DC/DC}}$ is set to zero, then power losses during DC/DC conversion are not taken into account in (24). Similarly, if the weighting factor $w_{\text{losses}}^{\text{DC/AC}}$ is considered equal to zero, then power losses during DC/AC power conversion are neglected in (24).

Voltage deviations: In the proposed framework, voltage deviations outside an operation band can also be penalised. This way, the DSO can indirectly control the voltage profile of the ADN. The operation band is defined by an upper ($\overline{V}$) and a lower limit $\underline{V}$, respectively. These limits are imposed by the DSO. Note that $V^{\min} < \underline{V}$ and $\overline{V} < V^{\max}$. The extra cost related with voltage deviations in the *i*th network bus can be described as

$$C_i^{\text{VD}} = \begin{cases} 0, & \text{if} \quad \underline{V}^2 \le \left|\mathscr{U}_i\right|^2 \le \overline{V}^2, \\ w_i^{\text{VD}}\left(\left|\mathscr{U}_i\right|^2 - \overline{V}^2\right), & \text{if} \quad \left|\mathscr{U}_i\right|^2 \ge \overline{V}^2, \\ w_i^{\text{VD}}\left(\underline{V}^2 - \left|\mathscr{U}_i\right|^2\right), & \text{if} \quad \underline{V}^2 \ge \left|\mathscr{U}_i\right|^2, \end{cases}$$

where w_i^{VD} is a weighting factor that is adjusted by the DSO. Using this weighting factor, the DSO can penalise in a different way the voltage deviations in different network buses. This way, the DSO can penalise the voltage deviations in network buses that are critical for the voltage control of the ADN. The overall voltage deviation cost function is defined as

$$C^{\text{VD}} = \sum_{i\,\in\,\mathscr{V}} C_i^{\text{VD}}. \tag{29}$$

Note that if C_i^{VD} is equal to zero $\forall i \in \mathscr{V}$, then voltage deviations are not penalised and not included in the cost function (24).

Using the proposed weighting factors the DSO can easily modify (24). Additionally, it is important to note that the proposed objective function has a generic form. Thus, several DSO-defined cost terms can be readily integrated in (24).

Step 4. Computation of the individual inertia constants: At this step, the individual power injections, i.e. P_k^{IR}, and the maximum permissible value of the ROCOF, $\text{ROCOF}_{\max}$, are used to determine the individual inertia constants, i.e. H_k, of all DRESs. This is done by using (30), which directly derived from (7)

$$H_k = \frac{f_n(P_k^{IR}(pu) - P_k^{ss}(\text{pu}))}{2 \times \text{ROCOF}_{max}}, \quad (30)$$

Step 5. Dispatch of DRESs: The new H_k values are forwarded to the corresponding DRESs and the algorithm terminates. Recall that the values of H_k remain constant during the time period considered. Thus, power injections are determined by the actual (measured) ROCOF values, ROCOF_{meas}, as

$$P_k(pu) = \frac{2H_k}{f_n}\text{ROCOF}_{meas} + P_k^{ss}(\text{pu}) \quad (31)$$

6 Method evaluation

In this section, the proposed algorithms are evaluated using simulation results acquired from a benchmark distribution grid. The examined test system is presented in Section 6.1. In Section 6.2, simple scenarios are presented to better highlight several distinct aspects of the proposed algorithms as well as to provide a better understanding concerning their implementation. Section 6.3 investigates the impact of forecast errors on the performance of the proposed methods. Finally, in Section 6.4 time-series simulations for a whole day are conducted assuming variable generation and loading conditions. Different sizes for the UCs are also considered. The evaluation of the results and the comparison of all cases provide useful insights concerning the inertial capability of ADNs.

6.1 System under study

The developed algorithms are validated on the European MV benchmark grid introduced by the CIGRE in [20]. The grid is depicted in Fig. 5. The nominal voltage and frequency of the grid are equal to of 20 kV and 50 Hz, respectively. The maximum ampacity of power lines is considered equal to 416 A. All other model parameters can be found in [32].

6.2 Explanatory examples

This section presents some indicative scenarios in order to better demonstrate the functionalities of the proposed algorithms. For this purpose, only four DRESs is initially installed in the grid. Note that no loads are considered. The rated power and the location of all DRESs are depicted in Table 1. In this Table, the power provided by the primary source ($P_{g,k}$) of all DRESs is also presented. T_{max} for all converter switches is considered equal to 175°C.

The sizing inertia constant of all DRESs, i.e. $\tilde{H}_k$, is considered equal to 6 s. This value is used since it corresponds to the average inertia constant of continental Europe nowadays [4]. Additionally, according to the recent standards [33, 34], the ROCOF that DRESs shall at least be capable of withstanding is equal to 2.5 Hz/s. Based on these information, $E_{UC,k}^{max}$ and $P_{UC,k}^{max}$ are computed. The results are presented in Table 1.

Under these assumptions, the inertial capability of the ADN is computed using Algorithm 1. Initially, a power flow analysis is performed to determine the power that flows through the PCC during the steady-state operation. According to the results, $P_0^{ss} = 1037.33$ kW. Afterwards, the optimisation problem of (21) is solved to determine the injections of UCs and to evaluate the maximum power that can be delivered at the PCC, i.e. P_0^{IRmax}. The total extra power that can be provided by the UCs during a frequency event is equal to 651.2 kW. Detailed information concerning the contribution of each UC are provided in Table 2. Due to power losses in converters and grid lines, total power of $P_0^{IRmax} = 1676.20$ kW is delivered at the PCC. Note that a further increase of this power cannot be achieved due to technical and operational constraints.

In particular, as shown in Table 1, prior to the frequency event DRESs located at buses 6 and 9 operate very close to their rated power, producing 90 and 495 kW of real power, respectively. Thus, the temperature of the corresponding IGBTs is equal to 151.2 °C. This value is very close to T_{max}. Therefore, to ensure that temperature violations are efficiently avoided, the proposed method

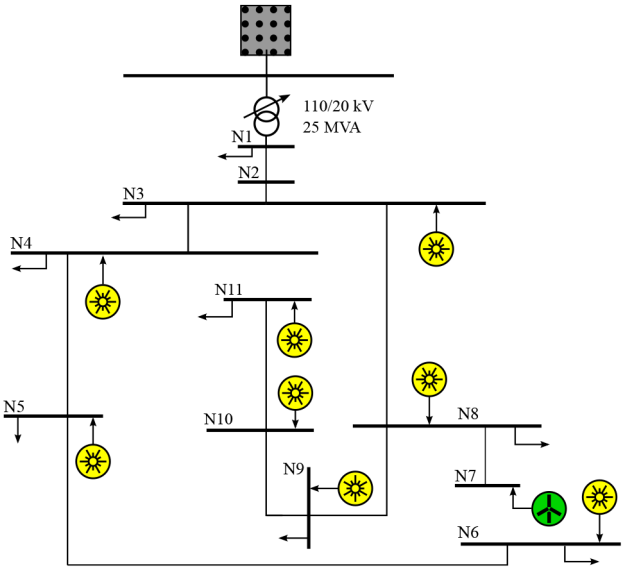

Fig. 5 *System under study*

Table 1 Parameters for the DRESs, used in Section 6.2

Reference	Bus	$S_{n,k}$	$P_{g,k}$	$P_{UC,k}^{max}$	$E_{UC,k}^{max}$
		kVA	kW	kW	kWh
G5	5	100	10	60	0.1
G6	6	100	90	60	0.1
G9	9	550	495	330	0.55
G10	10	550	450	330	0.55

Table 2 UC maximum injections

DRES	G5	G6	G9	G10
$P_{UC,k}$	60.00	40.18	221.01	330.00

Table 3 Temperature of IGBTs during steady-state operation (T_{IGBT}^{ss}) and after the inertial response (T_{IGBT}^{IR})

DRES	G5	G6	G9	G10
T_{IGBT}^{ss}	49.22	151.20	151.20	134.69
T_{IGBT}^{IR}	74.66	174.77	174.77	166.87

limits the contribution of the corresponding UCs during a frequency event to 40.18 kW and 221.01 kW, respectively. Recall that $P_{UC,k}^{max}$ for these UCs is 60 kW and 330 kW, respectively. On the other hand, UCs of the DRESs located at buses 5 and 10 can provide their maximum power, since temperature limits are not reached. These results are summarised in Table 2 and 3.

Once P_0^{IRmax} has been evaluated, the remaining task is to compute the H_{ag}^{max} value via (20). To convert P_0^{IRmax} and P_0^{ss} into p.u., a base power equal to 1300 kVA is used. This value corresponds to the total sum of the rated power of all installed DRESs. In Fig. 6, the H_{ag}^{max} of the ADN is plotted assuming different ROCOF values. Using these results, the TSO can estimate the maximum aggregated inertia constant of the ADN based on the desired maximum ROCOF withstand capability of the DRESs.

Now, let us assume that the TSO requests a maximum ROCOF withstand capability for all DRESs equal to 2.5 Hz/s. In this case, results of Fig. 6 indicate that H_{ag}^{max} is equal to 4.91 s. To demonstrate Algorithm 2, we assume that the TSO conducts contingency analysis, using the framework of [28], and requests a H_{ag}^{TSO} value equal to 4.5 s. This value is lower compared to the maximum inertial capability of the ADN. Thus, the DSO should optimally dispatch DRESs to provide this new inertia constant. For this purpose, (22) is used and the power that must be delivered at the

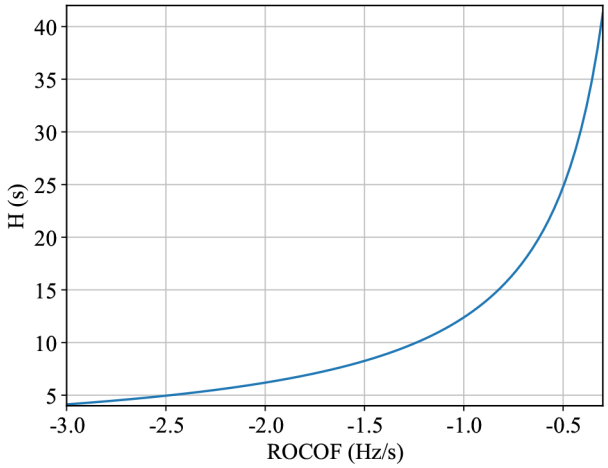

Fig. 6 *Aggregated inertia constant of the ADN under different ROCOF values*

Table 4 Results of the optimal allocation of inertia problem

Scenario	DRES	Bus 5	Bus 6	Bus 9	Bus 10	$\sum_{\forall k} P_{\mathrm{UC},k}$, kW
S1	$P_{\mathrm{UC},k}$	59.88 kW	40.01 kW	220.67 kW	275.33 kW	595.89
	H_k	5.99 s	4.00 s	4.01 s	5.01 s	
S2	$P_{\mathrm{UC0},k}$	59.56 kW	38.77 kW	210.15 kW	287.55 kW	596.03
	H_k	5.96 s	3.88 s	3.82 s	5.22 s	
S3	$P_{\mathrm{UC},k}$	60.00 kW	40.05 kW	221.00 kW	274.96 kW	596.01
	H_k	6.00 s	4.01 s	401 s	5.00 s	

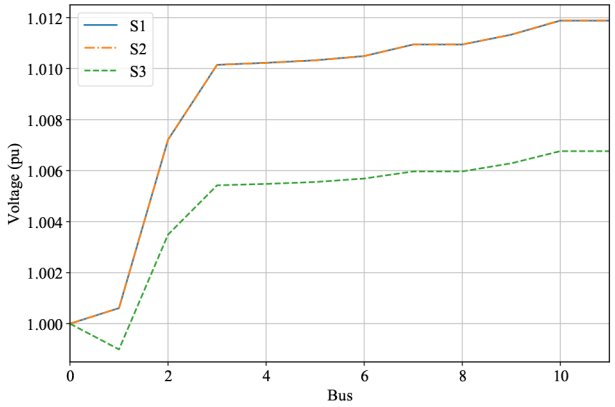

Fig. 7 *Voltage profiles for the three examined scenarios*

PCC is computed. In particular $P_0^{\mathrm{IR}} = 577.33$ kW. Afterwards, this power is distributed among DRESs using (23) and (24). Considering the weighting factors of (24), three scenarios are examined

• S1: This scenario aims to minimise line extra losses. Thus, the following weighting factors are considered

$$w_{\mathrm{losses}}^{\mathrm{line}} = 1 \text{ and } w_{\mathrm{lossses}}^{\mathrm{DC/DC}} = w_{\mathrm{lossses}}^{\mathrm{DC/AC}} = w_i^{\mathrm{VD}} = 0.$$

• S2: This scenario aims to minimise converter extra losses. In this case

$$w_{\mathrm{lossses}}^{\mathrm{DC/DC}} = w_{\mathrm{lossses}}^{\mathrm{DC/AC}} = 1, \text{ while } w_i^{\mathrm{VD}} = w_{\mathrm{losses}}^{\mathrm{line}} = 0.$$

• S3: In this scenario voltage deviations are penalised. The weighting factors are

$$w_i^{\mathrm{VD}} = 1, \text{ while } w_{\mathrm{lossses}}^{\mathrm{DC/DC}} = w_{\mathrm{lossses}}^{\mathrm{DC/AC}} = w_{\mathrm{losses}}^{\mathrm{line}} = 0.$$

The inertia constants for the three scenarios as well as the corresponding UC power injections are summarised in Table 4. In all examined scenarios, the power delivered at the PCC is equal to 577.33 kW. In the first scenario, line losses are minimised. Therefore, in this scenario the total power provided by the UCs of the four DRESs is lower compared to other cases. In the second scenario, converters losses are minimised. DRESs that operate close to their rated power present higher converter losses due to increased temperatures. Therefore, these units minimise their contribution to the inertial response. Finally, in the third scenario, voltage deviations are penalised. Therefore, DRESs modify their injections and consume reactive power to regulate voltage. The voltage profiles, along the feeder, for the three examined scenarios are presented in Fig. 7, verifying that in the third scenario the minimum voltage deviations are observed.

6.3 Impact of forecast errors

In this section the impact of forecasts errors on the performance of the proposed method is investigated. For this purpose, the following assumptions are considered: grid of Section 6.2 is used. It is assumed that TSO requests a $H_{\mathrm{ag}}^{\mathrm{TSO}}$ value equal to 4.5 s. The individual inertia constants, H_k, of the four DRESs are set according to scenario *S*2. The corresponding values are presented in Table 4.

The following analysis is performed: five different ROCOF values are considered, namely 2.5, 2.0, 1.5, 1.0 and 0.5 Hz/s. For each ROCOF value, a set of 10,000 simulations is conducted. In each simulation forecast errors concerning DRES production are considered. Forecast errors for each DRES fit a normal distribution with mean zero and standard deviation equal to 2.5%. Thus, in the 95% of the cases, the forecasting errors are <5% of the true values. For each simulation the power injection of all DRESs are calculated using (31) and the overall power injection at the PCC is computed in order to determine the aggregated inertia constant of the ADN.

Due to forecast errors, the aggregated inertia constant of the ADN cannot be always equal to 4.5 s, i.e. the value required by the TSO. This is also verified in Fig. 8, where the aggregated ADN inertia constant for all the examined cases is plotted. As shown, aggregated inertia values fit a normal distribution. The mean value of this distribution is equal to 4.5090 s, while the standard deviation is equal 0.3439 s. This implies that for a 95% confidence

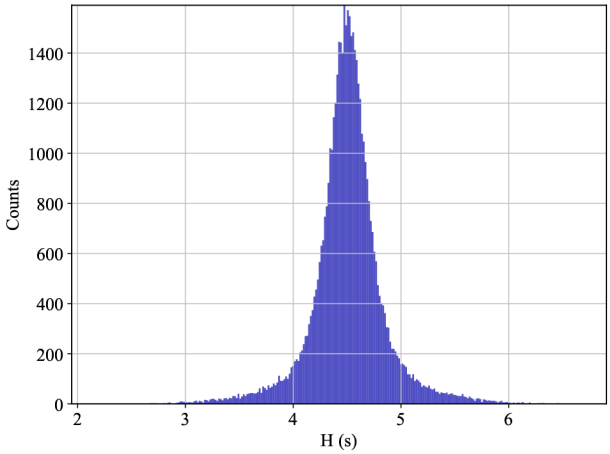

Fig. 8 *Histogram of the inertia constant at the PCC*

Table 5 Parameters of the DRESs, used in Section 6.3

Reference	Bus	Type	$P_{n,k}$ (kW)	$P^{\max}_{\mathrm{UC},k}$ (kW) Case 1	$E^{\max}_{\mathrm{UC},k}$ (kW) Case 1	$P^{\max}_{\mathrm{UC},k}$ (kW) Case 2	$E^{\max}_{\mathrm{UC},k}$ (kW) Case 2
GP3	3	PV	400	240	0.4	80	0.13
GP4	4	PV	400	240	0.4	80	0.13
GP5	5	PV	600	360	0.6	120	0.2
GP6	6	PV	600	360	0.6	120	0.2
GWT7	7	Wind	14250	8550	14.25	2850	4.75
GP8	8	PV	600	360	0.6	120	0.2
GP9	9	PV	600	360	0.6	120	0.2
GP10	10	PV	750	450	0.75	150	0.25
GP11	11	PV	200	120	0.2	40	0.06

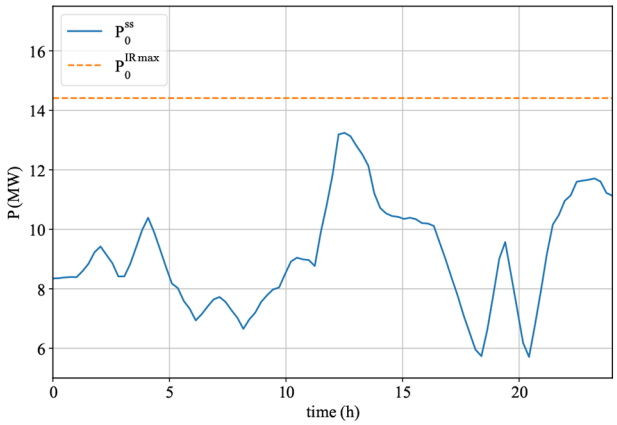

Fig. 9 *Case 1: Active power at the PCC during the steady-state operation and during the inertial response*

interval inertia values vary from 3.8212 to 5.1968 s. Thus, it can be concluded that forecast errors lead to degradation in the performance of the proposed method.

6.4 Time series simulations

In this section, the inertial capability of the ADN, depicted in Fig. 5, is evaluated for a whole day, using time-series simulations. The rated power for the installed loads can be found in [20], while the rated power and the type of the installed DRESs are presented in Table 5. Load demand and generation of the ADN change every 15 min based on the time-varying profiles presented in [32]. The profiles of [32] are scaled to the rated power of the DRESs.

Two distinct cases are considered regarding the sizing of the UCs. In the first one, UCs are sized assuming a maximum ROCOF withstand capability equal to 2.5 Hz/s and a sizing inertia constant equal to 6 s. In the second case, the sizing inertia constant is set to 2 s. The energy capacity, as well as the maximum discharging rate of the UCs for both cases are presented in Table 5.

6.4.1 Case 1: Initially, a power flow calculation is performed for each time instant to obtain the power that flows through PCC during the steady-state operation. This power is depicted in Fig. 9 with the blue curve. Afterwards, for each time instant, the optimisation problem of (21) is solved to determine the maximum power that can be delivered at the PCC without violating technical and operational constraints. This power is presented with the orange dotted curve in Fig. 9. As shown, for all instances, P_0^{IRmax} remains constant and it is limited to 14.41 MW. This limit corresponds to the current limit of the grid. Note that no other limiting factors such as temperature violations or overvoltages occur during the simulated period.

Recall that the difference between the two curves of Fig. 9 defines the power that can be provided by the UCs as an inertial response. This power varies considerably during the day. Therefore, the overall inertial capability of the ADN is also time-varying. This is further highlighted in Fig. 10, where the aggregated inertia constant of the ADN is plotted, assuming different values for $\mathrm{ROCOF}_{\max}$. It is worth pointing out that around $t = 12$ h, the inertial capability of the ADN is considerably limited and the corresponding inertia constant is lower than 2 s. Indeed, during this period, DRESs inject a high amount of active power that is exported to the transmission system. This increased production is also verified in Fig. 9. Thus, if a frequency event occurs during this high generation period, the DSO must limit the inertial response of UCs to ensure that all operational constraints of the grid are fulfiled. This limitation can be easily achieved since this response is fully programmable and can be adjusted remotely. To demonstrate Algorithm 2, it is assumed that TSO sets a limit for the maximum permissible ROCOF equal to 2 Hz/s and requests an aggregated inertia constant for the examined ADN equal to 80% of the maximum one. Note that the maximum aggregated inertia constant of the ADN during the day is presented in Fig. 10. Using these values, and (22), the DSO estimates the equivalent active

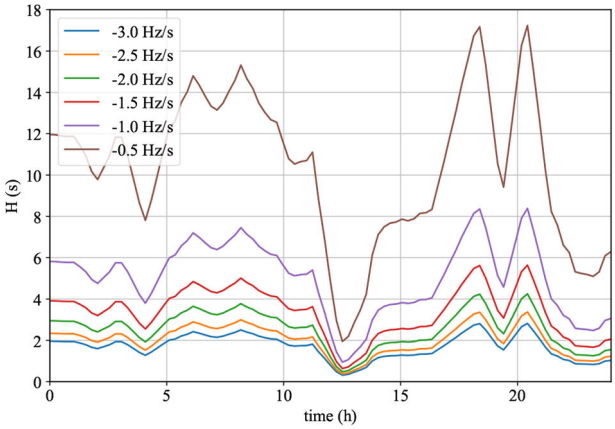

Fig. 10 *Case 1: Maximum aggregated inertia constant at the PCC, considering different values for* $ROCOF_{max}$

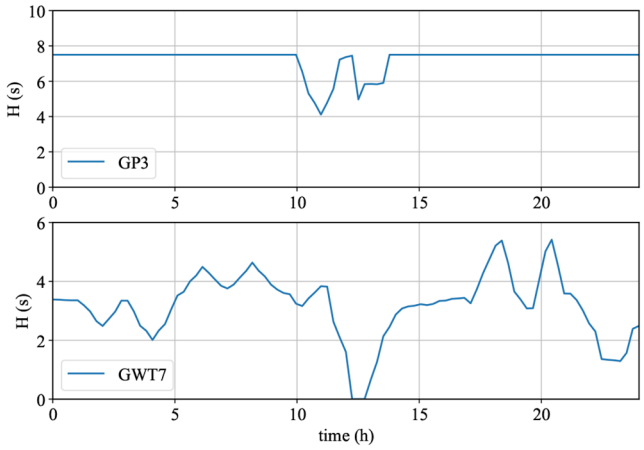

Fig. 11 *Inertia constants for GP3 and GWT7*

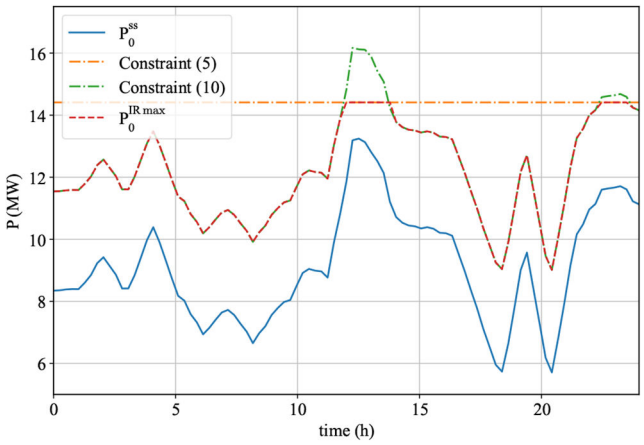

Fig. 12 *Case 2: Active power at the PCC during the steady-state operation and during the inertial response. Constraints (5) and (10) are also plotted*

power injection at the PCC, P_0^{IR}. Subsequently, (23) is evaluated for all time instants. In this case, all cost terms defined in (24) are considered of the same importance. Therefore, all weighting factors are set to 1, i.e. $w_{losses}^{line} = w_{lossses}^{DC/DC} = w_{lossses}^{DC/AC} = w_i^{VD} = 1,\ \forall i \in \mathcal{V}$.

The inertia constants obtained for generators GP3 and GWT7 are depicted in Fig. 11. As shown, during the high generation period, GP3 provides a limited contribution to the inertial response, while GWT7 do not contribute at all to the inertial response due to operational constraints. Similar remarks are also valid for all other DRESs. However, at this point, it is important to note that the use of UCs allows DRESs to provide an inertial response during the whole day. For instance, GP3 has an inertia constant that varies during the day from 4.0 to 7.8 s.

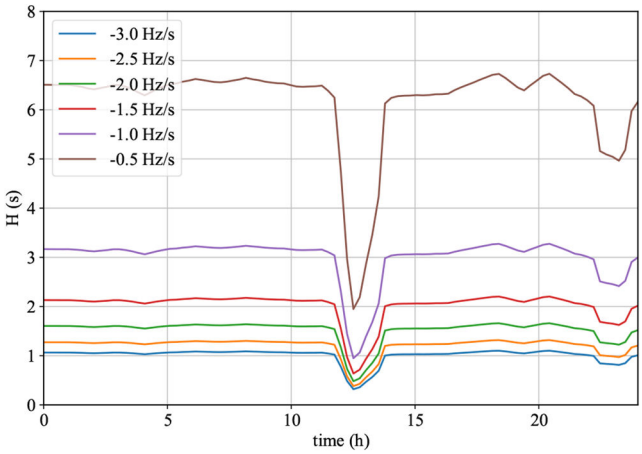

Fig. 13 *Case 2: Maximum aggregated inertia constant at the PCC, considering different values for* $ROCOF_{max}$

6.4.2 Case 2: In this subsection, the impact of the UC size on the inertial capability of the ADN is assessed. For this purpose, the analysis of Section 6.4.1 is repeated assuming that the UCs have a lower energy capacity, which presented in Table 5.

The corresponding results are depicted in Figs. 12 and 13. In particular, the pre-disturbance steady-state power is presented in Fig. 12 with the blue curve. In the same figure, the maximum power that can be delivered at the PCC during a frequency event is plotted alongside with constraints (5) and (10). As shown, the inertial capability of the ADN is mainly limited by the maximum discharging rate of the UCs, i.e. constraint (10). Only during high generation periods, for instance around $t = 12$ h, the inertial capability of the grid is restricted due to current limits, i.e. (5).

The maximum aggregated inertia constant of the ADN is presented in Fig. 13, assuming different values for $ROCOF_{max}$. As explained previously, most of the time UCs are able to provide their maximum power. Hence, the aggregated inertia constant of the ADN is almost constant during the day. In fact, the aggregated inertia constant is significantly reduced only when the injections of UCs are restricted due to the current constraints. It is worth mentioning that during these time, the aggregated inertia constant is identical to the one derived in case1.

Summarising, based on the presented results it can be concluded that the aggregated inertia constant of the ADN is determined by the extra power that UCs can provide during a frequency event and grid constraints. Higher sizes of UCs denote higher stored energy that can be utilised during frequency events to provide inertial support to the transmission system. Thus higher values for the aggregated inertia constant of the ADN can be generally achieved if all grid constraints are satisfied. This can be perceived by the comparisons of the results presented in Figs. 10 and 13. However, it should be noted that grid constraints may significantly reduce the aggregated inertial capability of the ADN. For instance, around 12 o'clock the aggregated inertia constant for

both the examined cases is limited to values lower than 2 s due to current constraints. Indeed, during this time instant, the extra power of the UCs of case 1 cannot be utilised. Thus, both case 1 and case 2 result in the same aggregated inertia constant.

The computational burden of the proposed framework is quantified by calculating the required execution time. The average execution time for each time instant for case 1 and case 2 is 69.41 and 73.8 s, respectively. This time is required to solve both problems, namely the evaluation of the maximum inertial capability of the ADN and the optimal inertia allocation. All simulations have been conducted using an i5-7200, 2.71 GHz, 8 Gb RAM personal computer. This relatively low execution time reveals that the proposed framework can readily support real-time applications in small MV networks.

7 Discussion and conclusions

As the penetration of DRESs increases, the total system inertia decreases due to the decommissioning of conventional SGs, jeopardising the overall system stability. In this context, new inertia sources must be deployed. A promising solution is the interconnection of DRESs to the utility grid via VSCs, which can provide a true inertial response to the system by utilising energy that it is stored on a local storage system. In this paper, UCs are selected as the local storage systems, since they can be used to provide, apart from the inertial response, and other ASs to the grid, e.g. high-frequency power smoothing, injection of controllable fault currents etc.

The inertial response of DRESs that are connected to the utility grid via VSC is fully configurable since the corresponding inertia constants can be remotely adjusted using control signals. In this context, DSOs can operate their grids as VPPs in order to participate in future frequency markets and provide an inertial response as AS to the transmission system. To participate in these markets, DSOs should be able to estimate with high accuracy the maximum inertial capability of their grids. Additionally, they should be able to appropriately dispatch DRESs in order to provide specific, TSO-defined inertial response.

To facilitate the implementation of the above-mentioned tasks, a new framework is developed in this paper. The proposed framework is based on a two-stage procedure that requires the interaction and communication between the TSO and the DSOs. In the first stage, DSOs evaluate the maximum aggregated inertial capability of their grids. Subsequently, this information is forwarded to the TSO, which determines, based on contingency analysis and market signals, the inertial response that each DSO shall provide to the transmission system. Then, the second stage begins and DSOs optimally dispatch DRESs to provide the inertial response requested by the TSO.

To implement these stages, two new methodologies are developed. The first one aims to determine the maximum aggregated inertial capability of ADNs, while the second one aims to optimally dispatch DRESs in order to provide specific, TSO-defined inertial response with the minimum cost. Both methodologies are developed based on OPF formulations and take into account all technical and operational limitations of ADNs. These limitations are incorporated as constraints in the OPF formulations and include current and voltage limits of the grid, UC limitations as well as temperature limitations of power converters.

The proposed methods are evaluated on the European MV benchmark grid proposed by CIGRE. Initially, a simple test case is presented to better highlight several distinct aspects of the proposed methods and to provide a better understanding concerning their implementation. Additionally, the impact of forecasts errors on the accuracy of the proposed methods is quantified. The corresponding analysis reveals that high forecast errors have an adverse effect on the performance of the proposed methods. Finally, time-series simulations for a single day are conducted. Different cases are considered to highlight the impact of several parameters, such as the size of UCs, converter temperature limitations, line congestions, on the inertial capability of ADNs. The results verify that the proposed methods can maximise the inertial capabilities of ADNs by fully exploiting the operational limits of these grids.

Summarising, the proposed methods constitute valuable tools for DSOs, since they can be used to estimate and control the provision of inertial response from ADNs to the transmission systems, allowing this way the participation of DSOs in future inertia markets. Future work will be conducted to develop more detailed and sophisticated cost-functions that fully quantify the cost for the provision of inertial response as AS to the TSO. Additionally, future work will be performed to reduce the computational complexity of the proposed framework. For this purpose linearised implementations of the proposed methods will be developed. These implementations will be validated on laboratory environment.

8 Acknowledgments

This work is a part of and is supported by the European Union, Horizon 2020 project ‘EASY-RES’ with Grant Agreement: 764090.

9 References

[1] Lew, D., Bartlett, D., Groom, A., *et al.*: ‘Secrets of successful integration: operating experience with high levels of variable, inverter-based generation’, *IEEE Power Energy Mag.*, 2019, **17**, (6), pp. 24–34

[2] Smith, J., Clark, C.: ‘The future's energy mix: tHe journey to integration’, *IEEE Power Energy Mag.*, 2019, **17**, (6), pp. 19–23

[3] Matevosyan, J., Badrzadeh, B., Prevost, T., *et al.*: ‘Grid-forming inverters: are they the key for high renewable penetration?’, *IEEE Power Energy Mag.*, 2019, **17**, (6), pp. 89–98

[4] ENTSO-E: ‘High penetration of power electronic interfaced power sources and the potential contribution of grid forming converters’, Technical Report, 2019

[5] ENTSO-E: ‘Ten year network developement plan’, 2016

[6] Poolla, B., Bolognani, S., Dörfler, F.: ‘Optimal placement of virtual inertia in power grids’, *IEEE Trans. Autom. Control*, 2017, **62**, (12), pp. 6209–6220

[7] ENTSO-E: ‘System dynamic issues for the synchronous zone of continental Europe’, 2017

[8] Breithaupt, T., Herwig, D., Hofmann, L., *et al.*: ‘Report on systemic issues’. Deliverable D1.1 of EU H2020 project MIGRATE – Massive InteGRATion of power Electronic devices, December 2016

[9] ENTSO-E: ‘High penetration of power electronic interfaced power sources and the potential contribution of grid forming converters’. Guidance document for national implementation for network codes on grid connection reports from European Network for Transmission System Operators (ENTSO-E), 2017

[10] Ramasubramanian, D., Farantatos, E., Ziaeinejad, S., *et al.*: ‘Operation paradigm of an all converter interfaced generation bulk power system’, *IET Gener. Transm. Distrib*, 2018, **12**, (19), pp. 4240–4248

[11] Hirase, Y.: ‘Guidelines for required grid-supportive functions in grid-tied inverters with distributed energy resources’, *IET Energy Syst. Integr.*, 2019, **1**, (4), pp. 236–245

[12] Denis, G., Prevost, T., Debry, M., *et al.*: ‘The migrate project: the challenges of operating a transmission grid with only inverter-based generation. A grid-forming control improvement with transient current-limiting control’, *IET Renew. Power Gener.*, 2018, **12**, (5), pp. 523–529

[13] Yu, M., Roscoe, A., Booth, C., *et al.*: ‘Use of an inertia-less virtual synchronous machine within future power networks with high penetrations of converters’. 2016 Power Syst. Comput. Conf. (PSCC), Genoa, Italy, 2016, pp. 1–7

[14] Zhong, Q., Weiss, G.: ‘Synchronverters: inverters that mimic synchronous generators’, *IEEE Trans. Ind. Electron.*, 2011, **58**, (4), pp. 1259–1267

[15] Zhong, Q., Konstantopoulos, G., Ren, B., *et al.*: ‘Improved synchronverters with bounded frequency and voltage for smart grid integration’, *IEEE Trans. Smart Grid*, 2018, **9**, (2), pp. 786–796

[16] Alipoor, J., Miura, Y., Ise, T.: ‘Stability assessment and optimization methods for microgrid with multiple VSG units’, *IEEE Trans. Smart Grid*, 2018, **9**, (2), pp. 1462–1471

[17] Li, D., Zhu, Q., Lin, S., *et al.*: ‘A self-adaptive inertia and damping combination control of VSG to support frequency stability’, *IEEE Trans. Energy Convers.*, 2017, **32**, (1), pp. 397–398

[18] Alipoor, J., Miura, Y., Ise, T.: ‘Power system stabilization using virtual synchronous generator with alternating moment of inertia’, *IEEE Trans. Emerg. Sel. Topics Power Electron.*, 2015, **3**, (2), pp. 451–458

[19] Oureilidis, K., Malamaki, K., Gallos, K., *et al.*: ‘Ancillary services market design in distribution networks: review and identification of barries’, *Energies*, 2020, **13**, (4), p. 917

[20] CIGRETask Force C6.04.02: ‘Benchmark systems for network integration of renewable and distributed energy resources’. CIGRE, 2014

[21] Kundur, P.: ‘*Power system stability and control*’ (McGraw-Hill, New York, 1994)

[22] ABB: ‘Applying IGBTs’, 2009

[23] Infineon: ‘Thermal equivalent circuit models’, 2008

[24] Semikron: ‘Thermal resistance of IGBT Modules - specification and modelling’, 2014

[25] Mauricio, J., Barragan-Villarejo, M., Casanova Delgado, L., *et al.*: 'First report on the electric and thermal dynamic modelling of DRES/BESS'. Deliverable D2.2 of EU H2020 project EASY-RES - Enable Ancillary Services by Renewable Energy Sources, 2020
[26] ENTSO-E: 'Rate of change of frequency (ROCOF) withstand capablity'. Guidance Document for National Implementation for Network Codes on Grid Connection reports from European Network for Transmission System Operators (ENTSO-E), 2017
[27] Urdal, H., Ierna, R., Zhu, J., *et al.*: 'System strength considerations in a converter dominated power system', *IET Renew. Power Gener.*, 2015, **9**, (1), pp. 10–17
[28] ENTSO-E RG-CE System Protection and Dynamics Sub Group: 'Frequency stability evaluation criteria for the synchronous zone of continental Europe', Version 11, March 2018
[29] Seneviratne, C., Ozansoy, C.: 'Frequency response due to a large generator loss with the increasing penetration of wind/PV generation - A literature review', *Renewable and Sustainable Energy Reviews*, 2016, **57**, pp. 659–668
[30] Agranat, O., MacGill, I., Bruce, A.: 'Fast frequency markets under high penetration of renewable energy in the Australian national electricity market'. 2015 Asia - Pacific Solar Research Conf., Queensland, Australia, 2015
[31] Virtanen, P., Gommers, R., Oliphant, T.E., *et al.*: 'SciPy 1.0: fundamental algorithms for scientific computing in python', *Nature Methods*, 2020, **17**, (3), pp. 261–272
[32] Rudion, K., Orths, A., Styczynski, Z., *et al.*: 'Design of benchmark of medium voltage distribution network for investigation of DG integration'. IEEE Power Engin. Soc. Gen. Meet., Montreal, Que., 2006
[33] CLC/TS 50549-1: 'Requirements for generating plants to be connected in parallel with distribution networks – Part 1: connection to a LV distribution network above 16 A', 2015
[34] CLC/TS 50549-2: 'Requirements for generating plants to be connected in parallel with distribution networks - Part 2: Connection to a MV distribution network above 16 A', 2015